J Nanostruct 12(2): 316-329, Spring 2022

RESEARCH PAPER

Preparation and Characterization of Hierarchical CdS Nanoflowers for Efficient Photocatalytic Degradation

Kahlaa H. Aboud [1], *Selma M. H. AL-Jawad* [1]*, *and Natheer Jamal Imran* [2]

[1] *Applied physics department, School of Applied Sciences, University of Technology, Baghdad, Iraq*

[2] *Environment and Water Directorate, Ministry of Science and Technology, Baghdad, Iraq*

ARTICLE INFO

Article History:
Received 09 January 2022
Accepted 18 March 2022
Published 01 April 2022

Keywords:
CdS thin films
Deposition time
Hydrothermal method
Optical properties
Photocatalytic properties
Structural properties

ABSTRACT

Hierarchical Cadmium Sulphide (CdS) thin films with high-surface area were deposited on a glass substrate using a hydrothermal technique at various deposition periods' durations for the first time. As-deposited CdS films have been investigated structural, optical, morphological, and photocatalytic properties. The results demonstrate that the deposition period has a substantial impact on the physical and chemical characteristics of these films. X-ray diffraction (XRD) revealed that the structural characteristics of all samples are hexagonal and cubic phases. Field emission scanning electron microscopy (FE-SEM) reveals the development of hierarchical nanoflowers with tiny gaps at lower deposition times; nevertheless, the density of the nanoflakes rises as the deposition time increases. Atomic force microscope (AFM) images of the films indicate morphological alterations and an increase in surface roughness from 4.58 nm to 7.26 nm. In conjunction with different time deposition, the photoluminescence (PL) behavior of the samples is outstanding, with acceptable transmittance spectra in the visible range. The optical band gap is directly connected to the deposition conditions, according to the transmittance data analysis; a direct bandgap ranging from 2.34 to 2.17 e V was calculated. The nanoflowers cadmium sulfide films exhibited unprecedented photocatalytic activities for the decomposition of methyl blue (MB) and methyl violet (MV) dyes, because high surface area, low energy gap, and efficient charge separation properties for prepared films.

How to cite this article
Aboud K H, AL-Jawad S M H, and Imran N J. Preparation and Characterization of Hierarchical CdS Nanoflowers for Efficient Photocatalytic Degradation. J Nanostruct, 2022; 12(2):316-329. DOI: 10.22052/JNS.2022.02.009

INTRODUCTION

Cadmium sulfide (CdS) stands out among other materials because it is of the n-type photo-sensible semiconductor with a direct bandgap value of 2.4 eV at room temperature [1]. CdS can develop in two distinct structural phases depending on deposition conditions: hexagonal (wurtzite) and cubic (zinc blende) [2]. Direct bandgap thin-film cadmium sulfide (CdS) has received a lot of attention due to its intermediate bandgap, high absorption coefficient, good conversion efficiency, and stability[2,3]. It possesses attractive properties that allow it to be used in solar cell applications (where it is used as a window or buffer material) [4] , photoresistors, phosphors, electroluminescence[4] , diodes[5] , thin film transistors[6], and, photocatalysis [2]. CdS thin films have been favored for future applications

* *Corresponding Author Email: salma_aljawad@yahoo.com*

among the many metal sulfide chalcogenides due to their extensive availability and ease of manufacture [7]. Different approaches have been utilized by different researchers to generate CdS. These include spray pyrolysis[8], sputtering [9], vacuum evaporation [10], electrodeposition [11], chemical bath deposition [12], and hydrothermal [13]. Each technique has produced films with a wide range of characteristics that be tailored to a specific application. However, CdS thin films have been developed using a variety of techniques. Some of these methods are complex, while hydrothermal processing has many advantages such as high component purity, homogeneity, crystal symmetry, scale distributions, narrow particles, cost-effectiveness, high yield, and the potential to achieve a controlled morphology [14]. The influence of deposition time on the physical characteristics of CdS films has been studied in a few experiments utilizing various source materials. Among them are: Moualkia et al. [15] studied the effects of deposition time (15–90 min) and temperature (55–75 °C) on optical and structural properties of CdS thin films deposited by chemical bath deposition using cadmium sulfate (CdSO4) and thiourea ($CS(NH_2)_2$) as the primary sources of Cd and S atoms in the bath solution. In addition, Barote and his co-workers [16] investigated the influence of deposition duration from 30 to 90 minutes on the thickness of CdS thin films. They discovered that layer thicknesses are raised for 60 minutes and subsequently reduced.

In recent years, to solve the global energy shortage and environmental pollution by converting solar energy into chemical fuels with using photocatalytic semiconductor was studied. As photocatalysts based on semiconductors, cadmium sulfide has gotten a lot of attention because has a visible-lightresponsive photocatalyst with relatively narrow bandgap and appropriately negative potential of conduction band edge for proton reduction. Numerous studies have reported the fabrication of CdS thin films. However, a review of the literature shows the absence of reports on the characterization of hierarchical CdS thin films to define the structure, surface morphology, optical and photocatalytic properties of thin films using the hydrothermal method. Therefore, in this work, the structural, morphological, optical, and photocatalytic properties as a function of deposition time of CdS thin films have been studied. A photocatalytic activity has been determined to CdS hierarchical by testing methyl blue (MB) and methyl violet (MV) dyes under xenon radiation.

MATERIALS AND METHODS

Preparation of CdS hierarchical

Cadmium sulfide (CdS) films have been deposited with hydrothermal technique on glass substrates. Where the glass substrates were submerged for 8 hours in hydrochloric acid and then ultrasound cleaned with acetone and deionized water. First, 20 ml of 0.05 M ($3CdSO_4.8H_2O$) was added, was blended slowly with add NH_3 Ammonia constant agitation in order to change the pH value of the resolution to 12, by using a magnetic stirrer. Then, with a continuous stirring for 15 minutes, 20 ml of 0.1 M thiourea was applied. Finally, the resultant solution was put into a teflon container with such a glass substrate that was sealed inside the stainless steel autoclave for hydrothermal processing. The autoclave was sealed and held for (45 min, 1 h, and 2 h) at 150 °C. Then, the autoclave was cooled at room temperature. After that, the glass substrate was taken out and deionized water was used to clean it in an ultrasonic bath.

Characterizations

The crystal composition of the preparation CdS thin film was determined by X-ray diffraction analysis (XRD-6000, Shimadzu, Japan) with Cu Kα radiation (λ=1.54056 Å) for 2θ in a range from 20° to 80°. A Shimadzu UV-1800 spectrophotometer was used to perform UV-Visible spectroscopy in the wavelength range of 200-1100 nm. FLUORESCENCE (Varian) Hitachi Type S-4160 SN use of measurement photoluminescence: EL05043810. The topography of the surface was taken by AFM images (CSPM-5000). The Field Emission Scanning Electron Microscope (FE-SEM) was used to examine the surface, which works at (Zeiss sigma 300- HV).

Photocatalytic experiment of CdS thin films

In this study, CdS thin films were used as photocatalysts to study the degradation of methyl blue (MB) and methyl violet (MV) dye under a 40 mW Xenon light. The photocatalytic tests were carried out under the same conditions. To perform photocatalytic experiments, 0.01 mg of methyl blue or methyl valuate dye was dissolved in 1000 mL deionized water and stirred for 5 minutes. There was about a 15-centimeter distance,

between the source and the aqueous solution. The samples were exposed to illumination in the dye solution for up to 260 minutes for each sample. The reaction was maintained at room temperature. For 20-minute intervals, the absorbance of (MB) and (MV) solutions was monitored. Photocatalytic degradation of methyl blue (MB) and methyl violet (MV) was monitored, using a UV–Vis spectrophotometer with a twin beam in a wavelength range of 300–1000 nm (UV-1800 Shimadzu). The degradation process performance was measured as a function of time using absorption at maximum absorption = 660 nm for MB and 585 nm for MV. The photocatalytic elimination, a pseudo-first-order reaction, was quantified using the formula [17].

$$ln\frac{C}{C_0} = -Kt \quad (1)$$

Where C_0 represents the initial concentration of MB and MV (mg/l), C represents the concentration at each time interval in mg/l, (K) represents the rate constant, and t represents the irradiation time in minutes.

Removal (%) of methyl blue (MB) and methyl violet (MV) can be determined via the relation [17]:

$$Degradation\ (\%) = (\frac{C_0 - C}{C_0}) \times 100 \quad (2)$$

RESULTS AND DISCUSSION

Structural properties

CdS film can form with a cubic (zinc blende) or hexagonal (wurtzite) structure depending on the deposition parameters [18]. X-ray diffraction was used to evaluate the structural properties of the deposited CdS thin films. The X-ray diffraction spectra of hydrothermal CdS films formed at various times is shown in Fig. 1. As can be observed from the acquired diffraction patterns, a prominent peak at 2θ=26.7° may be ascribed to the H(002) /C(111) plane of cubic and hexagonal CdS, in addition to minor peak belong to hexagonal phase [19]. The intensity and sharpness of this peak increases as the deposition period increases, which is produced by improved crystallinity of the films. As shown in Fig.1, films show also diffraction peaks at 2θ = 44.1° with plane (220) and 2θ = 31.9 with plane (200), respectively, which correlate to CdS zinc-blende structure. These results well agree with the standard (JCPDS No. 42-1411). The average crystalline size was calculated from the X-ray diffraction pattern using Scherrer's formula [20] and it tabulated in Table 1. As the time of the

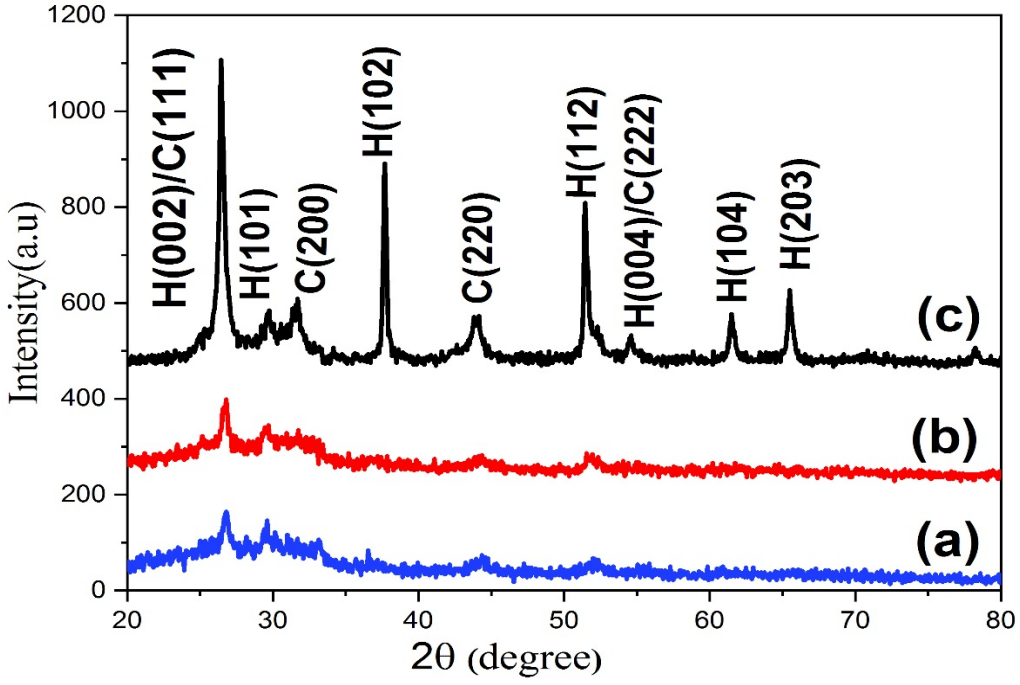

Fig. 1. XRD spectrum of CdS thin films under different deposition time (a) 45 min, (b) 1h and (c) 2h.

Table 1. Crystallite size, the position of diffraction peaks (2θ), FWHM, and lattice constants of CdS thin films synthesized at 150 ºC with various time.

CdS samples	Crystal structure	D (nm)	2(deg.) measured	(FWHM) (deg.)	Lattice constants (Å)		
					a=b	c	c/a
Pure CdS 45min	Hexagonal	6.544	26.533	0.73	4.1787	6.716	1.6071
Pure CdS 1h	Hexagonal	8.849	26.7006	0.495	4.1573	6.67204	1.6048
Pure CdS 2h	Hexagonal	10.746	26.547	0.4228	4.1017	6.7133	1.636
Standard	JCPDS card no .41-1049				4.14092	6.7198	1.6228

deposition rises, the crystalline size increases from 6.5 nm to 10.7 nm.

$$GS = \frac{A\lambda}{\Delta\theta cos\theta} \quad (3)$$

Where λ is the incident x-ray wavelength (1.5405 Å), A is the form factor (0.94), Δθ the peak location is defined as the total width at half maximum in radians and the angle value in radians. In addition, the following equation was used to calculate lattice parameters [21].

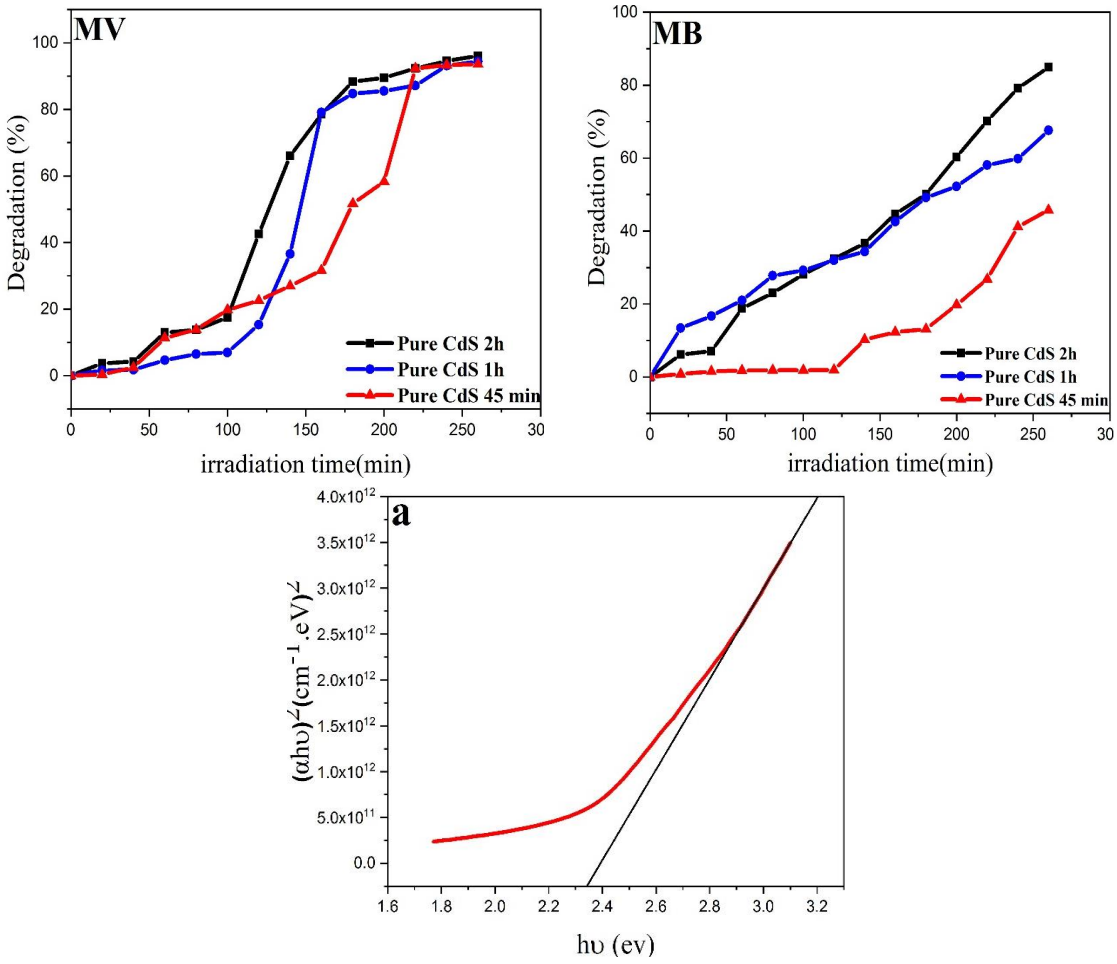

Fig. 2. Williamson-Hall (W-H) plot of CdS thin films with various time (a) 45 min CdS, (b) 1h CdS and (c) 2h CdS.

Table 2. Crystallite size, lattice microstrain values, and Dislocation density of CdS thin films

Sample	Gs (nm)	Gs (nm)	Dislocation density (δ X 10^{-3}) (Lines/nm^2)	Microstrain
	Scherrer method	W-H method		(Ɛ)
pure CdS 45 min	6.544	9.033	23.351	-0.0043
pure CdS 1h	6.365	14.1005	24.683	-0.0027
pure CdS 2h	10.746	18.55	8.659	-0.0018

$$\frac{1}{d^2} = \frac{4}{3}\left[\frac{h^2+hk+k^2}{a^2}\right] + \frac{L^2}{C^2} \quad (4)$$

Where d is the inter-planar distance, (h, k, l) is miller indices, and (a and c) are lattice constants. The Williamson–Hall (W–H) plot was used to calculate the strain in the samples. The strain contribution may be expressed as [22].

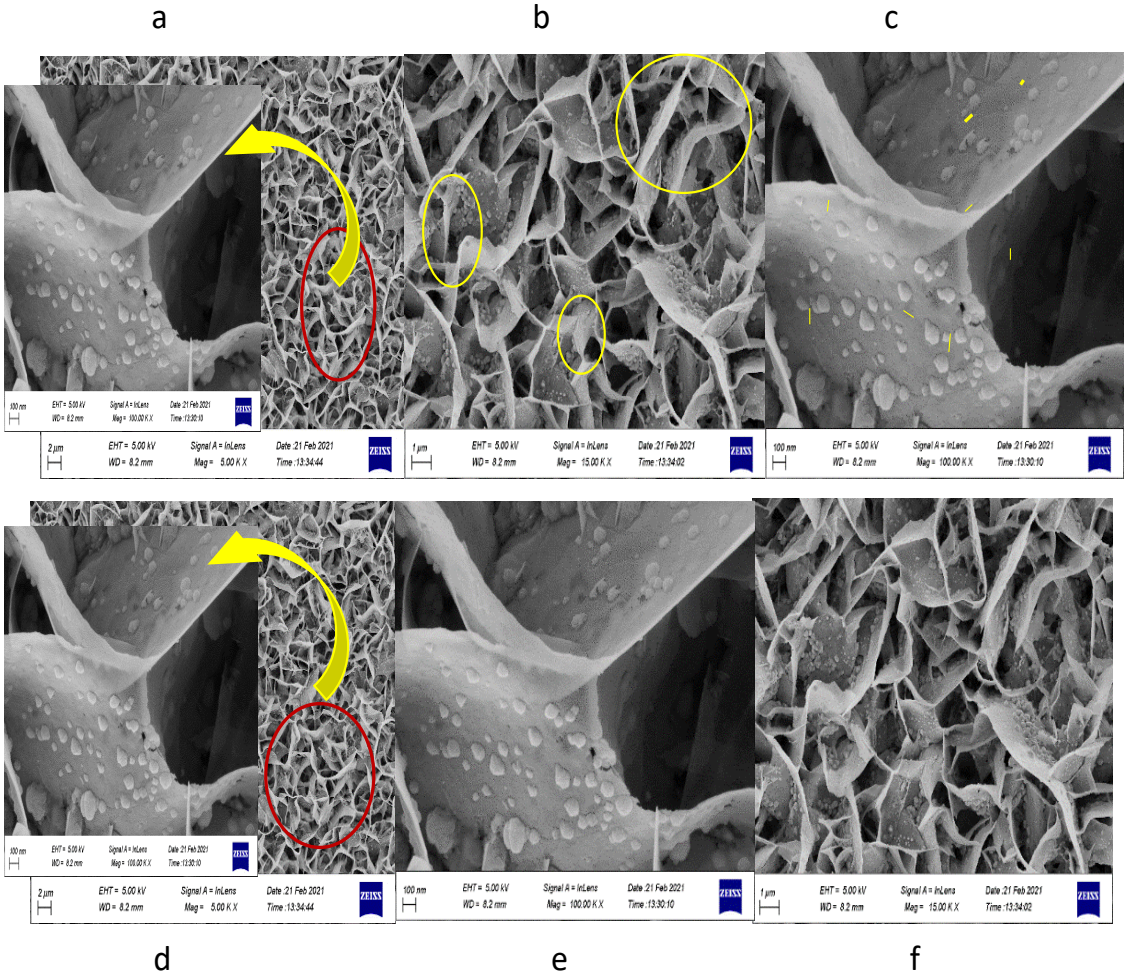

Fig. 3. FE-SEM images of CdS thin films with different time of 45 min (a, b, c), and 1h (d, e, f).

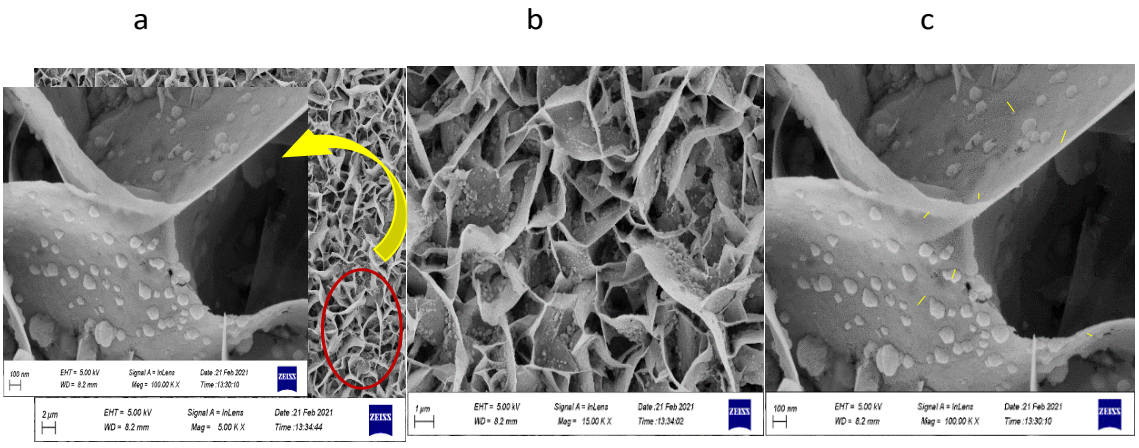

Fig. 4. FE-SEM images of CdS thin films with different time of 2h (g, h, m).

$$\beta_{hkl} = \beta_{GS} + \beta_{\varepsilon} \quad (5)$$

Where, β_{GS} and β_S the crystal deformation and defect caused diffraction line widening owing to lattice strain represents both the crystallite size widening and the strain-induced widening. The Debye–Scherrer formula may be used to calculate the diffraction line broadening owing to crystallite size. We can write equation (6) with the help of these broadening.

$$\beta cos\theta = 4\varepsilon sin\theta + \frac{k\lambda}{G_S} \quad (6)$$

Equation 6 describes the model of homogeneous deformation when it is presumed that every material characteristic is independent of measurement direction. Fig. 2 shows the graph of 4sin and βcosθ for pure CdS at 45 min, 1 h, and 2 h samples. As shown in Table 2, the crystalline size (GS) and microstrain (Ɛ) were determined from the slope of the prepared line and y-axis intersection, respectively. It may be assumed that the crystalline size values of the W-H diagram indicate that the crystalline size is more significant than in the Scheer reaction. A negative slope in the plot indicates the presence of compressive strain for all samples, which indicates that the CdS films got subjected to compressive microstrain.

Morphological Properties of CdS

FE-SEM

FE-SEM was used to characterize the morphologies and microstructures of the as-prepared CdS products. Figs. 3 and 4 show a typical FE-SEM picture of CdS deposited by hydrothermal technique at 150°C for 45 min, 1 h, and 2 h. It is apparent from the images that the surface morphology of the CdS sample deposited with 45 minute differs from that of the samples generated at a longer duration. Fig. 3 (a ,b, and c) show the typical FE-SEM image of the pure

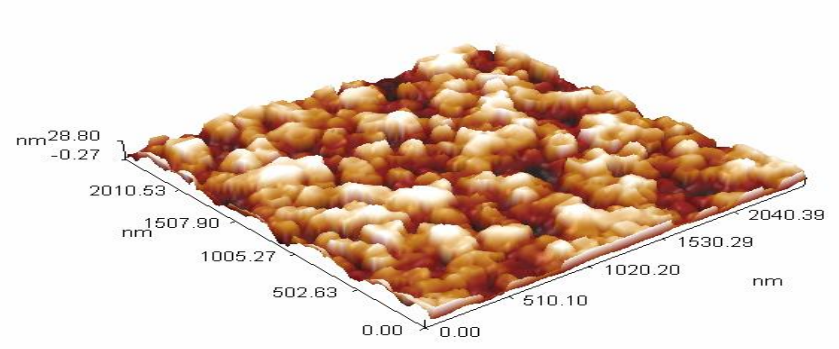

Fig. 5. FE-SEM cross-sectional images of the CdS films prepared by hydrothermal method with different time of a) 45 min, b) 1h, and c)2h.

Table 3. Grain size and surface roughness parameter values from AFM measurement for pure CdS thin films samples.

Samples	Grain size (nm)	Roughness Average (nm)	Root Mean Square (nm)
Pure CdS 45 min	64.42	4.04	4.58
Pure CdS 1h	66.51	6.11	7.26
Pure CdS 2h	87.76	4.58	5.3

CdS nanoflowers sample prepared at 45 min has hierarchical (shown as red line in Fig. 3 a) . A variety of flower-like structures has uniformly dispersed from which no other morphologies can be found, showing that this 3D nanostructure has a high yield (shown as yellow line in Fig. 3 b). As shown in Fig. 3 (d), the comprehensive morphological information of the nanoflowers is displayed in the cross section FE-SEM image. The hierarchical nanoflowers are made up of uniform nanosheets with width ranging from 8.64 nm to 55.37 nm. When the images with various deposition times are compared, it is evident that the uniformity and disparity of the samples are maintained, and the morphologies of the samples are still nanoflake, which is comprised of uniform nanosheets. FE-SEM images of Fig. 3(d, e, and f) demonstrate the CdS deposited for 1 h is nanoflower, it has begun to bloom (shown as red line in Fig. 3 d). The integrated big petals appear to have plate-like forms and have vertically overlapped each other to form the CdS material. Fig. 3e illustrates that when the reaction time was increased; the tiny spheres expanded and encircled the surface of the CdS as a nanosheet (shown in high magnification). Sample morphologies a 'hierarchical nanoflowers' pattern may be seen in samples prepared for 45 minute and 1 hour. Fig. 4(g, h, and m) for CdS prepared for 2 h shows the 'nanoflake' nanostructures can be considered as self-agglomeration of tangled nanoplates in the vertical direction (shown as red line in Fig. 4g). Because time is the sole variable in the deposition process, variations in surface morphology and crystal structure might be caused by it.

FE-SEM cross-sectional images of samples prepared for different times is shown in Fig. 5. Fig. 5a shows image for sample prepared for 45 min, and from image is evident a morphologies hierarchical nanoflowers' for thin film. And Fig. 5b shows CdS prepared for 1h, it is clear the CdS has formed as open nanoflowers'. While, as the time of deposition increased, the nanoflowers' become are more blooming (Fig. 5c).

Atomic Force Microscopy (AFM)

The surface morphology gives more information about the homogeneity of the structure the surface morphology of thin films in terms of root mean squared roughness (Rrms) was investigated using atomic force microscopy (AFM). Fig. 6 shows the atomic-force microscope images of the surface nanostructure of the CdS film deposited by the hydrothermal method. It is evident that the films have varying surface roughness, which appears to be depending on the time of deposition. Based on the data analysis, rms values calculated is 4.58, 7.26, and 5.3 nm for CdS thin films deposited for 45 min, 1h, and 2 h, respectively. The surface roughness of the thin film prepared for 45 minute may be shown to be minimal. However, increasing the duration of deposition causes a rise in roughness to a high of 6.11 nm at 1h, and then progressively falls to a minimum of 4.58 nm at 2 h. According to this finding, the increase in surface roughness with deposition time can be related to increscent in CdS grain sizes as indicated by FE-SEM micrographs. As a result, employing time deposition CdS may increase the optical quality of the films, which is directly proportional to roughness. Once again, the rms values follow the same pattern as the crystallite and grain sizes seen in XRD and FE-SEM analyses.

Optical properties

UV-Visible

A detailed examination of Fig. 7 show the optical transmittance spectra of hydrothermally formed CdS thin films after 45 minutes, 1 hour, and 2 hours of deposition. The poor transparency

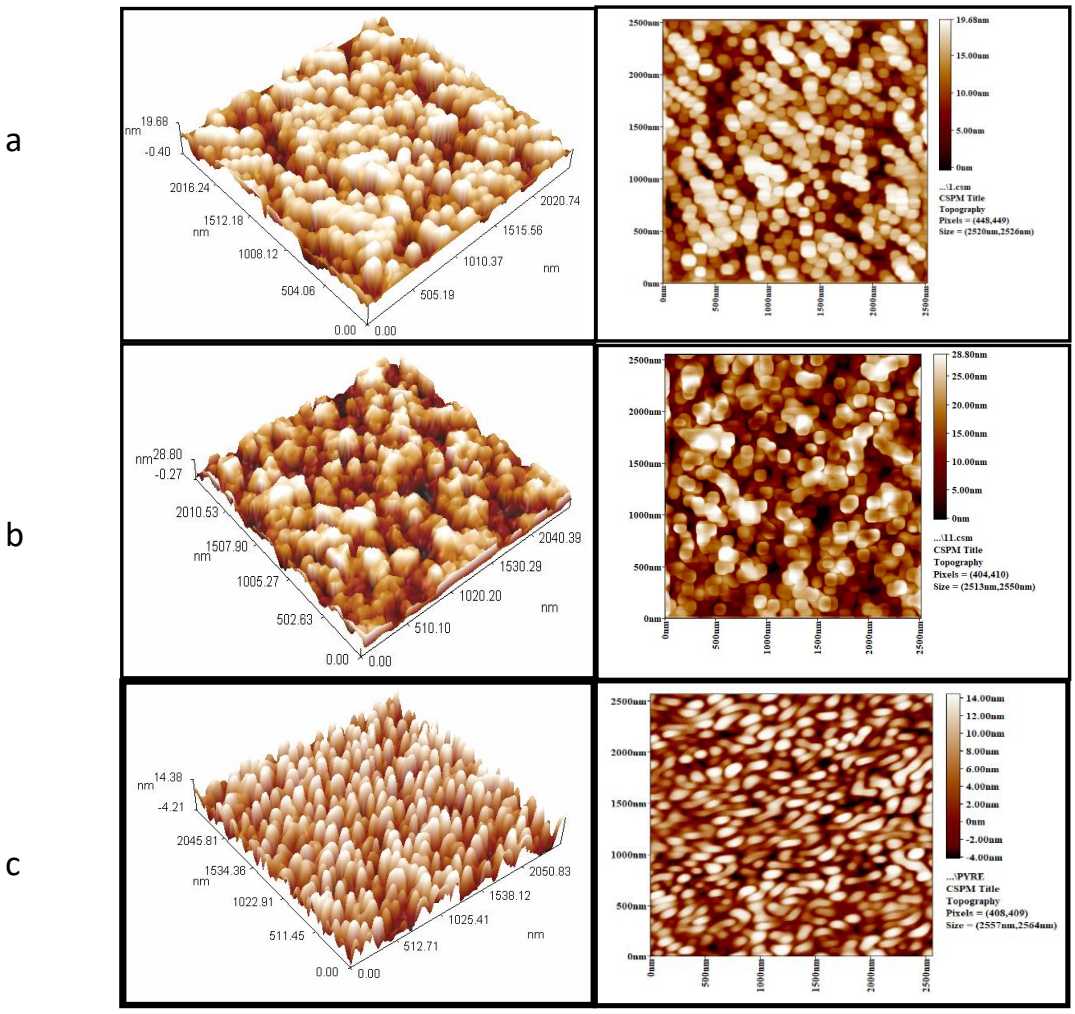

Fig. 6. (2D and 3D AFM image) of CdS thin film pure at different time. (a) 45 mint, (b) 1h and (c) 2h

of the sample developed at 1h might be attributed to the homogenous growth process's weakly adherent colloids as well as the film thickness. At deposition for 45 minutes, there is a maximum value transmittance. The absorbance (A) and thin film thickness (t) formulae were used to get the absorption coefficient (α) associated with the film's strong absorption region [23,24].

$$\alpha = 2.303\frac{A}{t} \quad (7)$$

The Tauc equation connects the absorption coefficient and the optical band gap (h⌡) [25,26].

$$\alpha h\nu = A(h\nu - E_g)^{1/2} \quad (8)$$

Where, 'hυ' is photon energy, 'Eg' is bandgap energy, 'A 'is a constant, 'n' is the exponential index that takes variable values depending on the type of the electron transition during the absorption process. The $(h\nu)^2$ versus (hν) plots of CdS films at various deposition times (45 min, 1h, and 2h), Fig. 8 depicts this. The optical band gap (Eg) is determined by extrapolating the linear part of the plot $(\alpha h\nu)^2$ versus (hν) in the abscissa (x-axis), indicating a direct optical transition. With increasing deposition periods of (45 minutes, 1 hour, and 2 hours), the CdS film's bandgap value was seen to decrease from 2.34 to 2.17 e V. Higher deposition time lead to formation of larger grain size, decreased the energy gap of the film.

Photoluminescence Spectroscopy

Photoluminescence spectroscopy was utilized

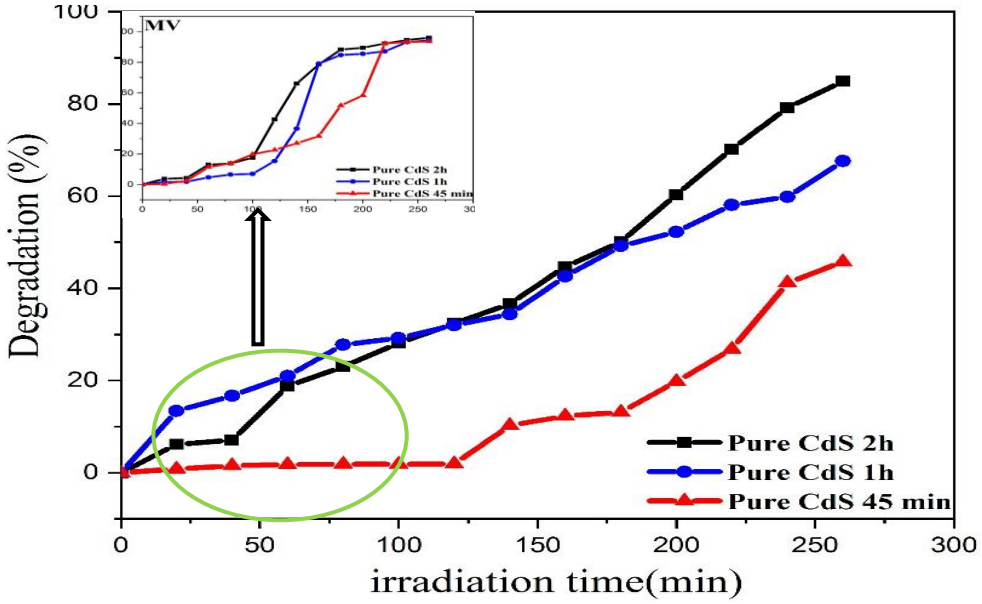

Fig. 7. Transmittance vs. wavelength plot of nanocrystalline CdS films for various time deposition

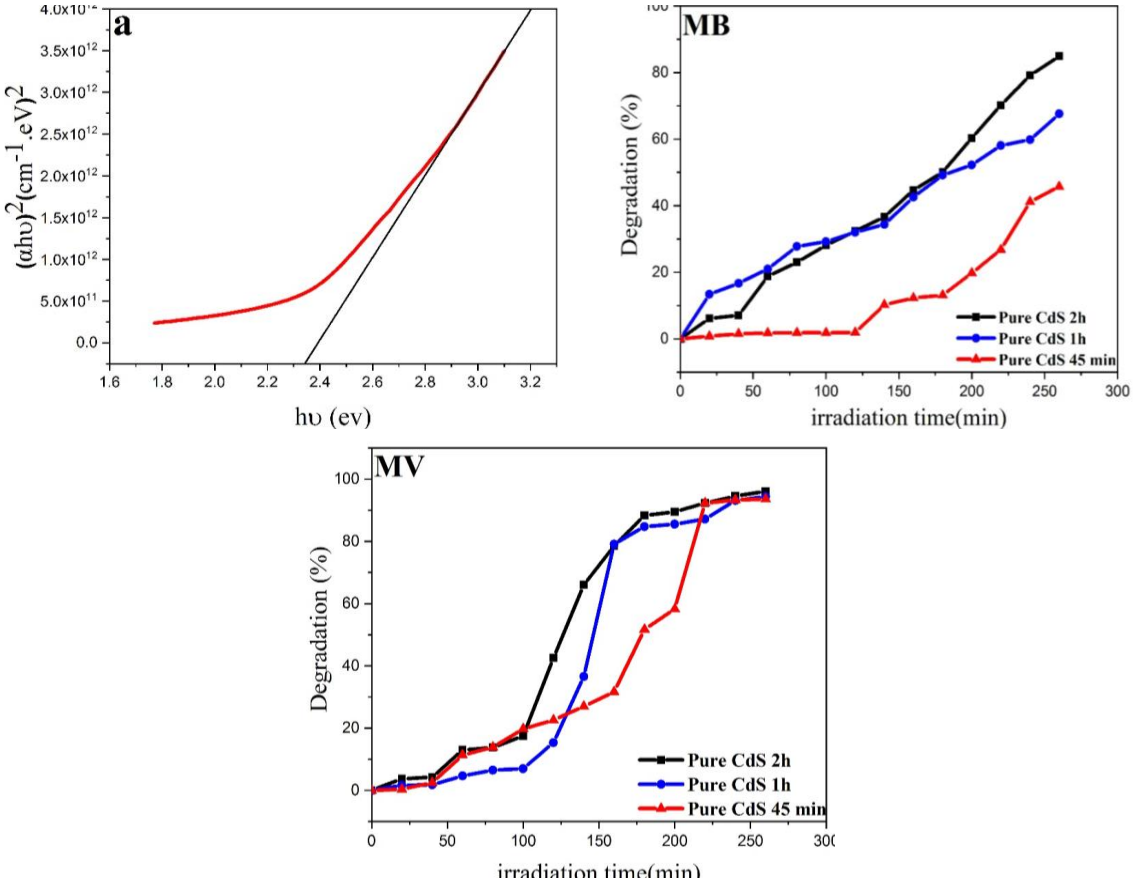

Fig. 8. Transmitted plots and bandgap of CdS thin films prepared at different time deposition (a) 45 min, (b) 1 h and, (c) 2 h.

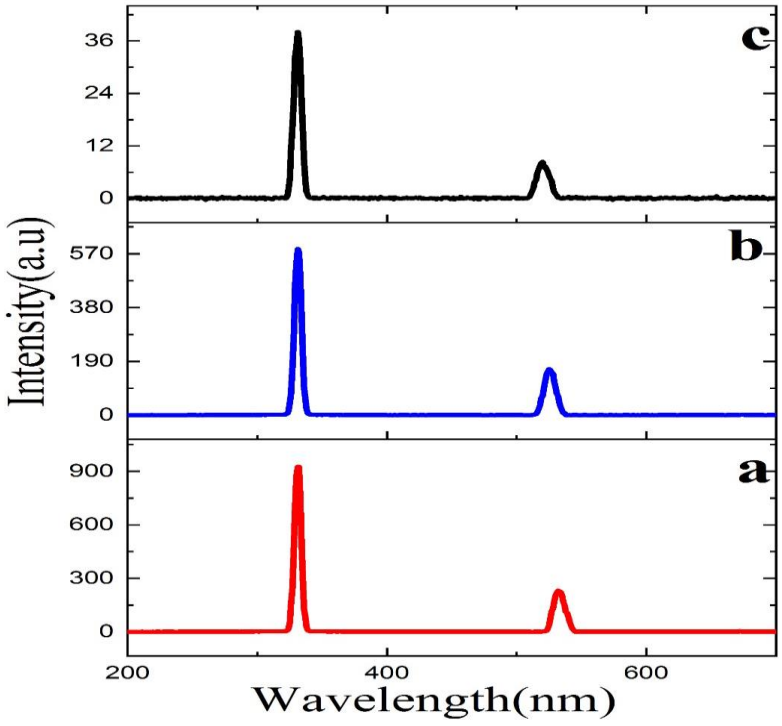

Fig. 9. PL spectra of CdS thin films prepared at different time: (a) 45 min

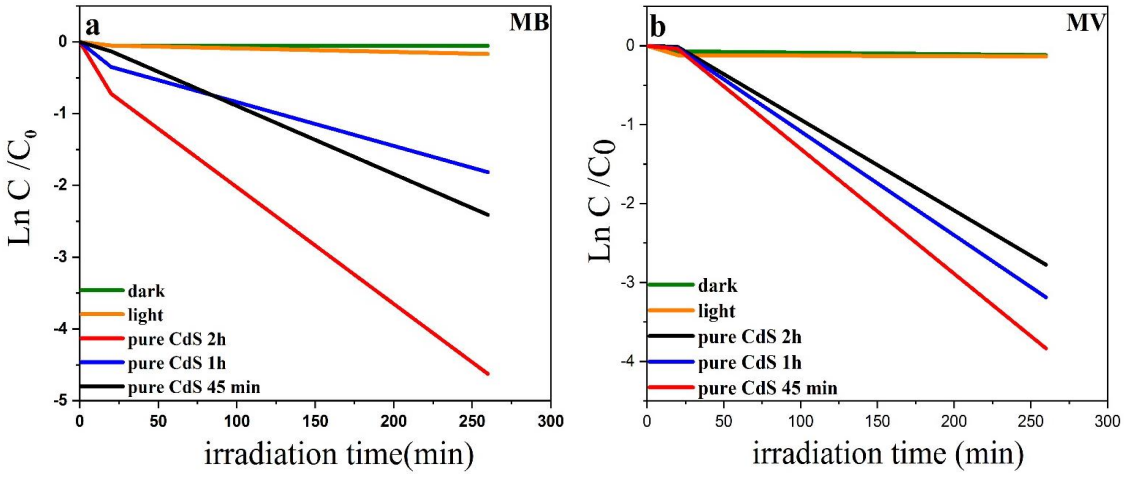

Fig. 10. Absorbance of an aqueous solution with an irradiation time of the CdS films immersed in (a) methyl blue (MB) and (b) Methyl violet (MV).

to look for crystalline disorder, interstitial vacancy, and band-to-band emission. The photoluminescence of CdS films were measured at room temperature using a 331 nm excitation wavelength. As shown in Fig. 9, the emission spectra of films exhibited a single wide peak that is located between 510 and 600 nm [27]. The emission peak of 520 nm (2.33 eV) for the pure CdS deposition for 45 min shows spectroscopy shifting. This is the same as the transmittance spectrum optical band difference. This finding is consistent with the above data in UV-VIS, as shown in Fig. 8. This emission occurred due to the recombination of a free conduction electron with

holes in the valence level and different reasons stated by [7]. While CdS deposited for (1h and 2h) have emission ranges at 525 nm (2.36 eV) and 539 nm (2.3), respectively, these are virtually similar to the transitional values for the energy gap values. The broadening of shape is due to the homogenous distribution of cadmium and sulfur atoms and the thermal energy associated with it.

Photocatalysis activity

In the case of visible light applications, chalcogenide has been known to be the most effective photocatalyst option. Semiconductors' photoreactivity is strongly sensitive to their morphology, crystal structure, phase composition, and shape [28]. The temporal dependence of optical absorbance of 0.01 for MB and MV solution was determined when kept in the dark and exposed to direct sunlight. The results conclusively demonstrate that whether exposed to direct sunlight or left in the dark, there was no significant difference in the absorbance of MB and MV solutions. The MB and MV degradation of as-synthesized photocatalysts was evaluated under

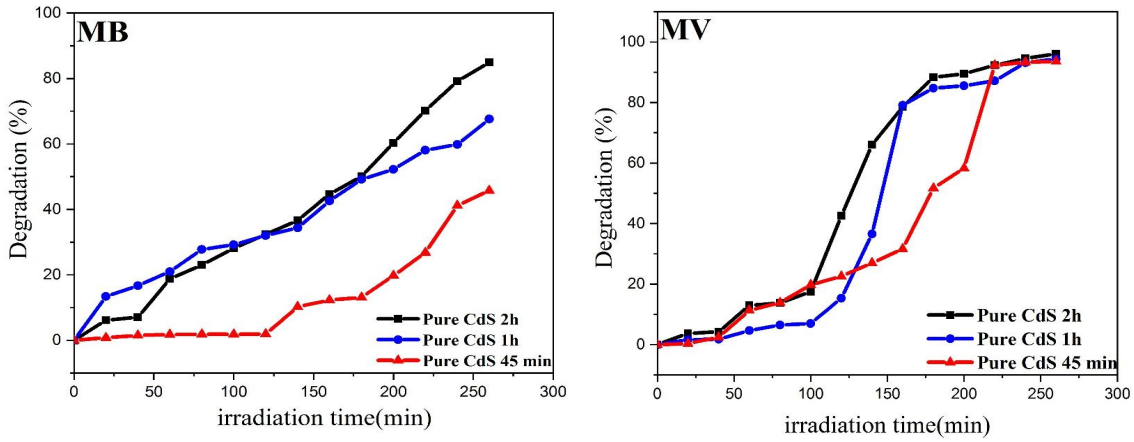

Fig.11. (Degradation of aqueous MB and MV solution as a function of irradiation light time of the CdS thin films immersed in it.

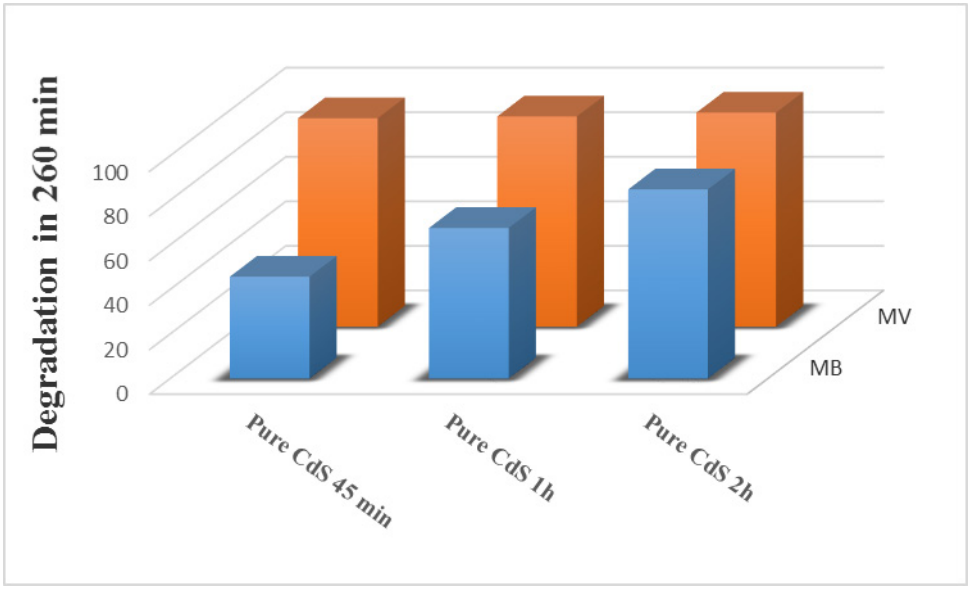

Fig. 12. Comparison between rate constants for photo degradation of pure CdS 2h , pure CdS 2h and pure CdS 45 min. Methyl Blue (MB), Methyl Violet (MV) (100 mg/l)

Table 4. Degradation and Rate constant (k) (%) of the methyl orange (MB), and methyl violet (MV) (100 mg/l) solution.

Samples	K min-1 for MB	Degradation in 260 min	K min-1 for MV	Degradation in 260 min
Pure CdS 45 min	0.01779	45.7424	0.01475	93.5811
Pure CdS 1h	0.00698	67.6109	0.01227	94.3805
Pure CdS 2h	0.00926	84.9307	0.01067	96.0991

the Xe lamp. The reaction begins, when electron-hole pairs appear on the CdS surface due to the absorption of light with an energy equals to or greater than the energy bandgap. The cadmium sulfide films electrons are reacted with methyl blue (MB) and methyl violet (MV). Where the OH• CdS radicals and holes are thought to be powerful oxidizing agents capable of degrading MB, and MV [29]. As the time of deposition increases, the energy gap of CdS films was decreased. This causes more photons to cross the energy gap, resulting in more (e-, h+) pairs being created and more OH being generated. This leads us to the conclusion that MB and MV decay accelerated was increased [30]. Fig. 10, show the UV–Vis absorbance spectra as a function of the photocatalytic reaction time in the presence of MB and MV dye aqueous solutions and degraded by CdS thin film. It can be observed that, with increasing irradiation duration, the intensity of the absorption peak at 663 nm for MB and 558 nm for MV gradually reduced. There is an improvement in the photocatalytic degradation of the MB and MV dyes; this can be related to many reasons such as higher specific surface area, surface morphology, crystal structure, surface roughness, and the films' improved photoresponse [31]. Fig. 11 (a, b) shows the photocatalytic degradation for MV and MB of pure CdS catalysts. Each run was carried out for 260 min. Although the degradation ratio of MV decreased slightly after each run, the CdS prepared with 2h exhibited efficient activity with about 84 % for MB of the degradation ratio. So, the CdS prepared with 2 h could remain has degradation ratio 96 % of MV of the initial activity after six runs. This is suggesting that the CdS prepared with 2h has higher degradation than other CdS prepared with 45 minte and 1 h. Table 4 shows the deterioration and the k values for MB and MV. It can be observed that the degradation increased with irradiation time. Further, it can be seen that the rate of increase in the degradation of pure CdS prepred with 2h thin films is significant. This may be attributed to the films becoming rough and porous and have a small grain size. Wu et al. [32] reported that 1D CdS/ hematite nanorods are with enhanced photocatalytic activity for MB degradation in comparison to the CdS nanowires.

Fig. 12 shows the comparison between rate constants for photodegradation of pure CdS prepared with 45 min, 1h, and 2h it was found that the rate of deterioration in pure CdS prepared with 2h was higher than the rate of deterioration of CdS prepared with 45 min and 1h. The probable reason is that bandgap width leads to an increase in the effective surface area, which leads to the increase of the photocatalytic activity. On the other hand, the bandgap for CdS prepared with 2 h is less than the bandgap for CdS prepared with 45 min and 1h, which leads to the increase of the photocatalytic activity for CdS prepared with 2 h.

CONCLUSION

The CdS was prepared using a low cost hydrothermal process. The effect of deposition time on the properties of CdS thin film was examined. The XRD patterns for CdS nanostructured thin film results displayed polycrystalline hexagonal wurtzite and cubic structure. It was observed that different deposition times of CdS played an important role in the crystallite size and lattice

constant. It was found that by increasing the time of deposition the intensity of all diffraction peaks increases. From FE-SEM, nanoflakes for CdS deposited for 2 h, while were found the nano flower constructed by numbers of nanoplates for CdS deposited for 45 min and 1 h. The AFM analysis results show that CdS thin films have rough and porous surface. UV-visible analysis showed all samples have a strong transition in the visible region. And it was observed that the energy gab decreasing with increase of deposition time. The photocatalytic activity of the pure CdS prepared at 2 h was enhanced compared to the pure samples prepared at 45 min and 1 h. The high photocatalytic activity of pure CdS prepared with 2h was attributed to low energy bandgap and high surface area.

CONFLICT OF INTEREST

The authors declare that there is no conflict of interests regarding the publication of this manuscript.

REFERENCES

1. Maghouli M, Eshghi H. Effect of deposition time on physical properties of nanostructured CdS thin films grown by chemical bath deposition technique. Superlattices Microstruct. 2019;128:327-333.
2. Li Y, Song Y-L, Zhou F-Q, Ji P-F, Tian M-L, Wan M-L, et al. Photovoltaic properties of CdS/Si multi-interface nanoheterojunction with incorporation of Cd nanocrystals into the interface. Mater Lett. 2016;164:539-542.
3. Cho SH, Kim SS, Park MH, Suh JH, Hong JK. Surface treatment of the window layer in CdS/CdTe solar cells. Journal of the Korean Physical Society. 2014;65(10):1590-1593.
4. Guduru S, Singh VP, Rajaputra S, Mishra S, Mangu R, St. Omer I. Characteristics of gold/cadmium sulfide nanowire Schottky diodes. Thin Solid Films. 2010;518(7):1809-1814.
5. Wondmagegn W, Mejia I, Salas-Villasenor A, Stiegler HJ, Quevedo-Lopez MA, Pieper RJ, et al. CdS Thin Film Transistor for Inverter and Operational Amplifier Circuit Applications. Microelectron Eng. 2016;157:64-70.
6. Mukherjee A, Ghosh P, Aboud AA, Mitra P. Influence of copper incorporation in CdS: Structural and morphological studies. Materials Chemistry and Physics. 2016;184:101-109.
7. Ilican S, Caglar Y, Caglar M, Yakuphanoglu F. The effects of substrate temperature on refractive index dispersion and optical constants of $CdZn(S_{0.8}Se_{0.2})_2$ alloy thin films. J Alloys Compd. 2009;480(2):234-237.
8. Moon B-S, Lee J-H, Jung H. Comparative studies of the properties of CdS films deposited on different substrates by R.F. sputtering. Thin Solid Films. 2006;511-512:299-303.
9. Sreekantha Reddy D, Narasimha Rao K, Gunasekhar KR, Dwarakanadha Reddy Y, Sreedhara Reddy P. Synthesis and dc magnetic susceptibility of the diluted magnetic semiconducting $Cd_{1-x}Mn_xS$ nanocrystalline films. J Alloys Compd. 2008;461(1-2):34-38.
10. Salim HI, Olusola OI, Ojo AA, Urasov KA, Dergacheva MB, Dharmadasa IM. Electrodeposition and characterisation of CdS thin films using thiourea precursor for application in solar cells. Journal of Materials Science: Materials in Electronics. 2016;27(7):6786-6799.
11. Cruz JS, Pérez RC, Delgado GT, Angel OZ. CdS thin films doped with metal-organic salts using chemical bath deposition. Thin Solid Films. 2010;518(7):1791-1795.
12. Loudhaief N, Labiadh H, Hannachi E, Zouaoui M, Salem MB. Synthesis of CdS Nanoparticles by Hydrothermal Method and Their Effects on the Electrical Properties of Bi-based Superconductors. Journal of Superconductivity and Novel Magnetism. 2017;31(8):2305-2312.
13. Judran HK, Yousif NA, Al-Jawad SMH. Preparation and characterization of CdS prepared by hydrothermal method. J Sol-Gel Sci Technol. 2020;97(1):48-62.
14. Moualkia H, Hariech S, Aida MS. Structural and optical properties of CdS thin films grown by chemical bath deposition. Thin Solid Films. 2009;518(4):1259-1262.
15. Barote MA, Yadav AA, Masumdar EU. Synthesis, characterization and photoelectrochemical properties of n-CdS thin films. Physica B: Condensed Matter. 2011;406(10):1865-1871.
16. Saikia L, Bhuyan D, Saikia M, Malakar B, Dutta DK, Sengupta P. Photocatalytic performance of ZnO nanomaterials for self sensitized degradation of malachite green dye under solar light. Applied Catalysis A: General. 2015;490:42-49.
17. Zhao XH, Wei AX, Zhao Y, Liu J. Structural and optical properties of CdS thin films prepared by chemical bath deposition at different ammonia concentration and S/Cd molar ratios. Journal of Materials Science: Materials in Electronics. 2012;24(2):457-462.
18. Soundeswaran S, Senthil Kumar O, Dhanasekaran R. Effect of ammonium sulphate on chemical bath deposition of CdS thin films. Mater Lett. 2004;58(19):2381-2385.
19. Al-Jawad SMH, Ismail MM, Ghazi SF. Characteristics of Ni-doped TiO_2 nanorod array films. Journal of the Australian Ceramic Society. 2020;57(1):295-304.
20. Al-Jawad SMH, Taha AA, Redha AM. Studying the structural, morphological, and optical properties of CuS:Ni nanostructure prepared by a hydrothermal method for biological activity. J Sol-Gel Sci Technol. 2019;91(2):310-323.
21. Williamson GK, Hall WH. X-ray line broadening from filed aluminium and wolfram. Acta Metall. 1953;1(1):22-31.
22. Al-Jawad SMH, Salman ON, Yousif NA. Influence of titanium tetrachloride concentration and multiple growth cycles of TiO_2 nanorod on photoanode performance in dye sensitized solar cell. Photonics and Nanostructures - Fundamentals and Applications. 2018;31:81-88.
23. Al-Jawad SMH, Salman ON, Yousif NA. INFLUENCE OF GROWTH TIME ON STRUCTURAL, OPTICAL AND ELECTRICAL PROPERTIES OF TiO_2 NANOROD ARRAYS DEPOSITED BY HYDROTHERMAL METHOD. Surf Rev Lett. 2019;26(03):1850155.
24. Al-Jawad SMH, Imran NJ, Mohammad MR. Effect of electrolyte solution and deposition methods on TiO_2-CdS core–shell nanotube arrays for photoelectrocatalytic application. The European Physical Journal Applied Physics. 2020;92(2):20102.
25. Taha AA, Al-Jawad SMH, Salim MM. INFLUENCE OF TITANIUM TETRAISOPROPOXIDE CONCENTRATION ON THE ANTIBACTERIAL ACTIVITY OF TiO_2 THIN FILMS. Surf Rev Lett.

2018;25(06):1850111.
26. Manthrammel MA, Ganesh V, Shkir M, Yahia IS, Alfaify S. Facile synthesis of La-doped CdS nanoparticles by microwave assisted co-precipitation technique for optoelectronic application. Materials Research Express. 2018;6(2):025022.
27. Talebian N, Nilforoushan MR, Ramazan Ghasem R. Enhanced photocatalytic activities of ZnO thin films: a comparative study of hybrid semiconductor nanomaterials. J Sol-Gel Sci Technol. 2012;64(1):36-46.
28. Shaban M, Mustafa M, El Sayed AM. Structural, optical, and photocatalytic properties of the spray deposited nanoporous CdS thin films; influence of copper doping, annealing, and deposition parameters. Mater Sci Semicond Process. 2016;56:329-343.
29. Shaban YA. Enhanced Photocatalytic Removal of Methylene Blue From Seawater Under Natural Sunlight Using Carbon-Modified n-TiO_2 Nanoparticles. Environment and Pollution. 2013;3(1).
30. Zheng G, Shang W, Xu L, Guo S, Zhou Z. Enhanced photocatalytic activity of ZnO thin films deriving from a porous structure. Mater Lett. 2015;150:1-4.
31. Wu J, Li Z, Li F. Synthesis and visible-light-driven photocatalytic activity of one-dimensional CdS/α-Fe_2O_3. Superlattices Microstruct. 2013;54:146-154.